8-1-2019

Probing Surface Characteristics of Rare Earth Minerals using Contact Angle Measurements, Atomic Force Microscopy, and Inverse Gas Chromatography

Mostafa Khodakarami

Lana Z. Alagha
Missouri University of Science and Technology, alaghal@mst.edu

Daniel J. Burnett

Recommended Citation

M. Khodakarami et al., "Probing Surface Characteristics of Rare Earth Minerals using Contact Angle Measurements, Atomic Force Microscopy, and Inverse Gas Chromatography," *ACS Omega*, vol. 4, no. 8, pp. 13319-13329, American Chemical Society (ACS), Aug 2019.
The definitive version is available at https://doi.org/10.1021/acsomega.9b01491

ACS OMEGA

Article

Cite This: ACS Omega 2019, 4, 13319−13329

http://pubs.acs.org/journal/acsodf

Probing Surface Characteristics of Rare Earth Minerals Using Contact Angle Measurements, Atomic Force Microscopy, and Inverse Gas Chromatography

Mostafa Khodakarami,[†] Lana Alagha,[*,†,‡] and Daniel J. Burnett[§]

[†]Department of Mining and Nuclear Engineering, Missouri University of Science and Technology, Rolla, Missouri 65409, United States

[‡]Thomas J. O'Keefe Institute for Sustainable Supply of Strategic Minerals, Rolla, Missouri 65409, United States

[§]Surface Measurement Systems, 2125 28th Street SW, Suite 1, Allentown, Pennsylvania 18103, United States

ABSTRACT: Rare earth minerals (REMs) such as bastnaesite, monazite, and xenotime are of considerable significance since they are the main commercial sources for rare earth elements (REEs) with cutting-edge applications. Fundamental understanding of surface properties of REMs is essential to identify the reactions taking place at different interfaces to develop more robust technologies for the recovery of REEs. The goal of this study is to provide a comprehensive investigation on the surface energy characteristics of bastnaesite and xenotime, as the primary sources of light and heavy rare earth elements, respectively. Crystal's orientation of REMs was identified using surface X-ray diffraction analysis, whereas the morphology and elemental composition were characterized using scanning electron microscopy and energy dispersive spectra analyses. Wettability of REMs was studied using sessile drop contact angle measurement technique, and the surface energy and its constituents were evaluated using Fowkes, van Oss−Chaudhury−Good, Owens−Wendt−Rabel−Kaelble, Zisman, and Neumann models. Atomic force microscopy (AFM) was used to compare the local surface properties and work of adhesion of REMs by analyzing the force profile between the mineral surfaces and a n-type silicon tip. Inverse gas chromatography (IGC) was employed to study the surface energy heterogeneity of REM powders and evaluate the dispersive and Lewis acid−base interactions. Results indicated that the dispersion forces have a larger contribution to the surface energy of both REMs in comparison with the polar interactions. The surface energy values obtained using contact angle measurements were lower than those obtained using IGC, however, the IGC results seemed to be closer to reality since the contact angle results showed a strong dependence on probe liquids, roughness, and local properties of the surfaces. Contact angle measurements and AFM analysis indicated that bastnaesite had higher hydrophobic character, whereas the IGC analysis revealed that the surface energy of xenotime was lower than that of bastnaesite at higher surface coverages. Despite the shortcomings of each method, results showed that a combination of these techniques could provide a deeper understanding of surface energy and wetting behavior of minerals.

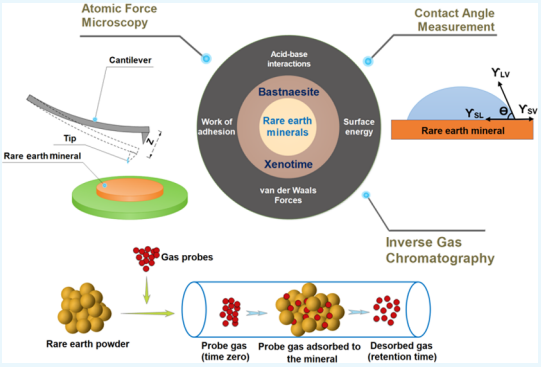

1. INTRODUCTION

The research in the field of rare earth elements (REEs) and their compounds is ongoing to better understand their physics and chemistry, which is essential to develop more efficient chemicals, reagents, and processes for the separation and recovery of heavy and light rare earth elements from host minerals. Beneficiation of rare earth minerals (REMs) and the consequent separation of REEs and their compounds have been very challenging at industrial scale due to their complex chemistries and similar physiochemical properties. Thermodynamic properties of surfaces and interfaces govern the response of rare earth minerals to a variety of separation processes such as froth flotation, dissolution, dispersion, flocculation, precipitation, and crystallization.[1−5] For example, in froth flotation process, minerals are separated based on the differences in their surface wettability, which influence the adsorption selectivity of reagents at solid/liquid/gas interfaces. This, in turn, has a significant impact on the particle−bubble attachment and, thus, the overall mineral recovery.[5−7]

Surface energy is the main property, which describes the wetting characteristics of mineral surfaces and the forces acting on them. It is considered as the amount of work required to make more of a surface. It is the phenomena that controls the hydrophobicity, reactivity, and polarity of minerals.[8−10] Conceptually, unfilled bonds at the edge of the solid and the effect of the nonadjacent molecules in the solid are key factors determining the total surface energy.[11] Two main components, namely, dispersion and polar, are usually considered for the

Received: May 21, 2019
Accepted: July 24, 2019
Published: August 6, 2019

DOI: 10.1021/acsomega.9b01491
ACS Omega 2019, 4, 13319−13329

calculation of total surface energy of solid materials.[12,13] The dispersion interactions result from long-range intermolecular forces caused by the interactions between electronic dipoles and induced dipoles in neighboring molecules or atoms.[12] The polar interactions are hydrogen-bonding, short-range interactions that are designated as Lewis acid−base or electron-donor/electron-acceptor reactions.[14] The nature of the chemical interactions taking place at the material surface is controlled by these surface energy constituents. Therefore, determination of the surface energy components of rare earth minerals, for example, can provide significant information, which will help to modify their surfaces for the purpose of designing more robust separation technologies.

Various techniques have been employed to assess the surface energy of minerals and other solid materials. Contact angle measurement is the most common technique used to analyze the wettability and surface energy of solid surfaces.[15] Contact angle measurement using direct optical method is advantageous because of its simplicity and the fact that only a small amount of probe liquids and small surface substrates is required. On the other hand, the small size of the liquid and substrate can increase the risk and impact of impurities on the contact angle.[16,17] Another serious limitation of the optical method is the inaccuracy of measurement as assigning a tangent line on the drop profile is uncertain when the contact angle is small (below 20°).[18] In addition, surface roughness and chemical heterogeneity could cause barriers to the motion of the three-phase contact line, which leads to the variation of contact angle values.[19,20] This chemical heterogeneity is due to the existence of impurities or functional groups on the surface, crystal orientation, and hydrophilic/hydrophobic sites on the surface. These can lead to energy heterogeneity and can largely affect the interactions between surfaces. Despite all advantages of this technique, such as its ability to investigate the surface energy of various crystalline faces, it is a macroscopic technique that gives an "average" surface property and does not present every specific site of nonideal mineral surfaces. Therefore, it is not applicable for powders with irregular shapes and varying surface area, porosity, and surface roughness.

Inverse gas chromatography (IGC) is a powerful technique for a more accurate evaluation of the anisotropic surface energy of powders and investigating the surface energy distributions of real materials.[21] This method is advantageous over conventional optical techniques since it avoids the effect of problems caused by surface roughness and morphology. However, IGC at infinite dilution conditions preferentially probes the sites with the highest energy.[22] The major limitation of IGC is the inability to distinguish the surface energy of individual crystalline face.

Recently, atomic force microscopy (AFM) has been used to investigate the surface energy of solid materials due to its capability of probing the surface interactions at molecular level.[23] The principle of surface analysis by AFM method is based on the measurement of the adhesion or pull-off force. Adhesion force is defined as the force required to pull the tip off the surface and is estimated by determining the deflection of the cantilever. The tip−sample interactions depend on the surface properties; therefore, the AFM results can be directly used to qualitatively evaluate and compare the surface energy of different materials.

All of the aforementioned methods have their own advantages and limitations, and no single method is sufficient for accurate assessment of surface energy. Despite all theoretical and experimental works performed to determine the surface energy of solid surfaces, only a few studies have been conducted to measure the surface energy of minerals, particularly rare earth minerals, which are the major focus of this paper. The majority of the published research work in this area has been devoted to study the hydrophobic characteristics of mineral surfaces and its impact on their floatability,[24,25] which is insufficient to draw an accurate conclusion about the surface energy since it ignored other important components that contribute to the total energy of a mineral surface. For example, several studies concluded that many sulfide minerals are floatable without using a collector due to the low degree of surface polarity and the large degree of hydrophobicity.[26] However, the surface oxidation and the possible hydrolysis of metal sulfides make it difficult to generalize the wetting analysis achieved by these studies.[24] Other researchers studied the surface properties of clay minerals where contact angle measurement and atomic force microscopy have been used to analyze the wetting characteristics.[27] However, results showed a large variation in surface properties as the clay minerals and layered silicates are anisotropic in nature.[28,29] Variation of surface energy values and its dependence on isomorphic substitution and mineral composition of clays have made the molecular dynamics simulation (MDS) an attractive tool for surface analysis of layered silicates.[30] However, MDS has been employed as a supportive tool for experimental techniques, although it can simulate different conditions and predict the surface characteristics. In the case of rare earth minerals, the data on surface characteristics is scarce. The flotation of bastnaesite and xenotime has been investigated, but the surface energy and its constituents has not been reported. Previous work focused on studying the surface chemistry of rare earth minerals in connection with the flotation process using ζ-potential measurements and analysis of reagents' adsorption on surfaces.[31−33] As concluded from the previous examples, there is a lack of reliable assessment of the surface energy of minerals, especially rare earth minerals. Therefore, the main objective of this study was to provide comprehensive investigations on the surface energy and wettability characteristics of two primary rare earth minerals; bastnaesite and xenotime, as the main commercial sources of light and heavy rare earth elements, respectively.

In this study, three powerful techniques have been used to determine and compare the total surface energy, and its polar and nonpolar components, of bastnaesite and xenotime: contact angle measurement, atomic force microscopy (AFM), and inverse gas chromatography (IGC). In addition, the orientation of crystal's of the two minerals was identified using surface X-ray diffraction analysis, whereas the morphology and elemental composition were characterized using field emission scanning electron microscope (FESEM) equipped with an EDAX energy dispersive system. The findings of this paper will provide a deeper understanding of the types of surface-active forces that govern the surface reactions of rare earth minerals, which is crucial to design more efficient chemicals, reagents, and processes for the separation and recovery of rare earth elements. To the bests of authors' knowledge, no such a comprehensive experimental study exists in the literature on the surface energy analyses of rare earth minerals.

2. EXPERIMENTAL SECTION

2.1. Materials. Two major rare earth minerals, bastnaesite and xenotime (as the main sources for light and heavy rare

DOI: 10.1021/acsomega.9b01491
ACS Omega 2019, 4, 13319−13329

earth elements), were used in this study. Bastnaesite $(REE)CO_2F$ and xenotime YPO_4 were obtained from Zagi Mountain in Pakistan and Bahia in Brazil, respectively. Both mineral samples were highly crystalline. The surface of mineral specimens was sequentially polished by 800, 1200, and 2400 grit silicon carbide grinding papers. When passing from one polishing paper to the next finer grade, the polished samples were immersed in and rinsed with acetone, ethanol, and deionized water to remove any traces of contaminants and polishing powder. This procedure was followed by drying the samples in the oven at 50 °C. Five probe liquids with known surface energy components were used for contact angle measurement and surface energy analysis: distilled water, formamide (>99.5%), ethylene glycol (99.8%), nitromethane (99.9%), and undecane (>99%), were purchased from Sigma-Aldrich (St. Louis, MO). The surface tension components of the used probe liquids are presented in Table 1.

Table 1. Surface Tension Components of the Probe Liquids Used in Contact Angle Measurements

	surface tension and the components (mJ m^{-2})				
probe liquid	γ_l^{lw}	γ_l^+	γ_l^-	γ_l^{AB}	γ_l
water	21.8	25.5	25.5	51	72.8
formamide	39	2.28	39.6	19	58
ethylene glycol	29	1.9	47	19	48
nitromethane	22			14.5	36.5
undecane	24.65				24.66

2.2. Methods. *2.2.1. Surface Characterization. 2.2.1.1. X-ray Crystallography.* The surface properties of a mineral can change depending on the crystallographic face studied. The surfaces of bastnaesite and xenotime used for contact angle measurements were first characterized by surface X-ray diffraction analysis for the determination of crystal face orientation. X-ray intensity data were collected using an X'PERT PRO diffractometer with Cu Kα radiation, Kα = 1.54439 Å. Data were recorded between 5 and 90 2θ with a scan step size of 0.03. The bastnaesite had a hexagonal structure with the space group $P\bar{6}2c$, whereas xenotime had a tetragonal structure with the space group $I41/amd$. Figure 1 shows the X-ray patterns of the rare earth crystals and the Miller indices of the surfaces used for contact angle measurement. The morphology of both minerals was dominated by {1 0 0} surfaces. Xenotime surface consisted of a regular rare earth oxides polyhedron accommodating small rare earth cations (yttrium and heavy rare earth elements). Bastnaesite consisted of two alternate layers of three rare earth fluorides and three carbonate groups.

2.2.1.2. Scanning Electron Microscopy and Energy Dispersive Spectroscopy (SEM–EDS). It is well known that the morphology of mineral surfaces has a strong effect on the contact angle measurements. Therefore, the morphology of rare earth mineral surfaces was examined at microscale using scanning electron microscopy (SEM). Hitachi S-4700 field emission scanning electron microscope (FESEM) equipped with an EDAX energy dispersive X-ray unit was used in this study since is capable to determine the chemical composition of the samples as well. The region evaluated with FESEM was analyzed with energy dispersion spectroscopy (EDS) to determine the specific elements that comprise the surface of the minerals. Figure 2 illustrates a relatively smooth topography of the surfaces with the roughness around 10 nm. The spectrum of X-ray intensity versus energy level indicated that yttrium and heavy rare earth elements (mainly erbium, gadolinium, and ytterbium) were the dominant rare earth elements of the xenotime surface. EDS analysis indicated that three light rare earth elements, namely, cerium, lanthanum, and neodymium were the dominant elements of bastnaesite surface.

2.2.1.3. Atomic Force Microscopy (AFM) Imaging. The surface topography of rare earth mineral surfaces was examined using a dual-probe atomic force microscope (DP-AFM). The AFM mapping was performed in contact mode using a VIT_P_C-A silicon cantilever (NT-MDT Spectrum Instruments) with force constant of 0.6–1 N/m and a pyramidal tip with the height of 15 μm. The scan was made over a 1 × 1 μm surface near the edge of the crystals where the three-phase contact line may take place in contact angle measurements (Figure 3). The samples were flat having irregularities around the edge; however, the surface roughness of bastnaesite was slightly larger than that of xenotime.

2.2.2. Wettability and Surface Energy Analysis. 2.2.2.1. Sessile Drop Contact Angle Measurements. Contact angle measurements were carried out on the surface of the polished and cleaned rare earth crystals by the sessile drop (solid/liquid/air system) method using a Ramé-Hart model 500 Advanced Goniometer. A drop of probe liquid was gently deposited at ambient conditions on the mineral surfaces using a microliter syringe, and the right, left and average angles were measured using the DropImage software. The measurements were repeated for four times, and the variation was in the range of ±(1–4) degrees. The obtained contact angles were used for surface energy analysis.

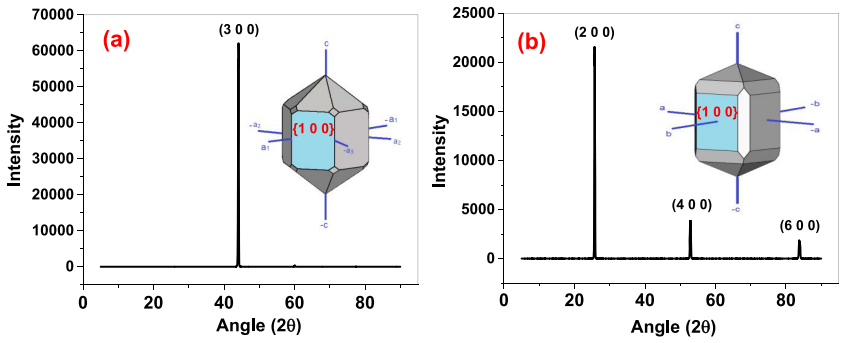

Figure 1. Surface X-ray diffraction spectra of (a) bastnaesite and (b) xenotime.

DOI: 10.1021/acsomega.9b01491
ACS Omega 2019, 4, 13319–13329

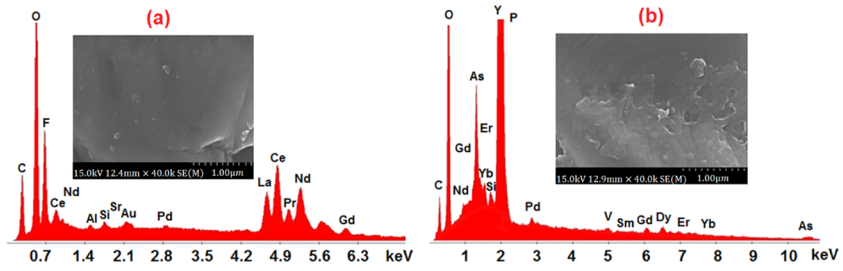

Figure 2. SEM image and EDS spectra of (a) bastnaesite and (b) xenotime.

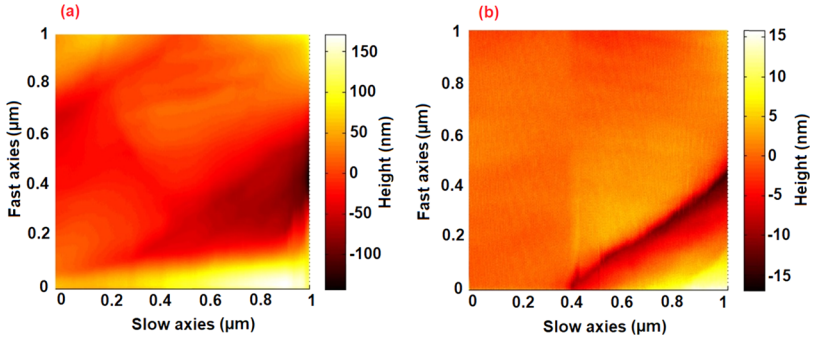

Figure 3. AFM topography maps of (a) bastnaesite and (b) xenotime.

2.2.2.2. Surface Energy Calculations by Contact Angle Measurement. The surface energy of solid surfaces can be evaluated by studying the wetting behavior of liquids on the solid sample. Wetting behavior is commonly studied by measuring the contact angle and the thermodynamic equilibrium between the liquid, solid, and gas or vapor phases (Figure 4).

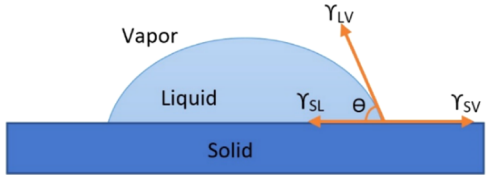

Figure 4. Schematic showing the relationship between contact angle and interfacial tensions.

Young proposed a mathematical expression, which correlates the contact angle θ with the surface energy of solid γ_s, the surface energy of liquid γ_l, and the interfacial energy γ_{sl}, between liquid and solid[34]

$$\gamma_s = \gamma_{sl} + \gamma_l \cos\theta \quad (1)$$

The problem with the Young equation is that the γ_s and γ_{sl} cannot be directly determined. In this regard, Dupre introduced the concepts of work of adhesion between phase a and phase b[35]

$$W_{ab} = \gamma_a + \gamma_b - \gamma_{ab} \quad (2)$$

If the phase "a" is solid and the phase "b" is liquid, then by substituting eq 1, the Young equation, into eq 2, the Young–Dupre equation would be obtained

$$W_{sl} = \gamma_l(1 + \cos\theta) \quad (3)$$

The work of cohesion of a solid or liquid can be similarly defined

$$W_{ss} = \gamma_s + \gamma_s - 0 = 2\gamma_s \quad (4)$$

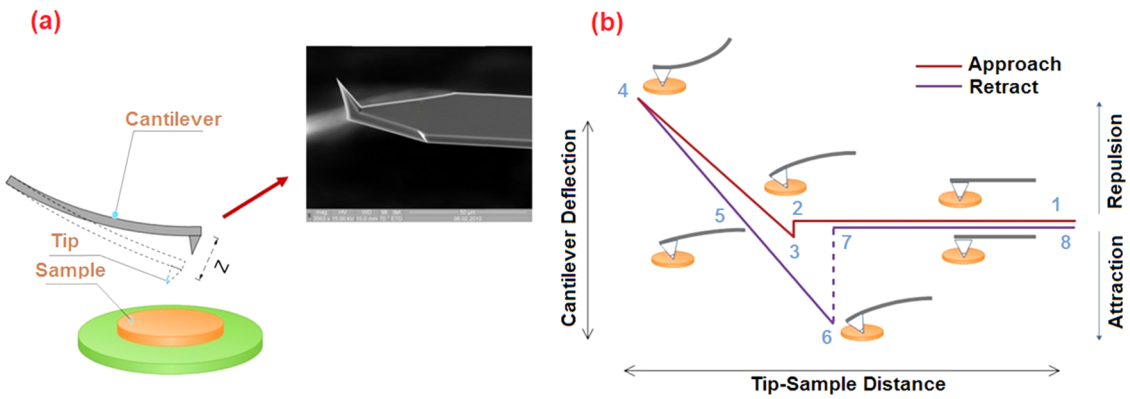

Figure 5. (a) SEM micrographs of the cantilever used in this study and a schematic showing the cantilever deflection; (b) a schematic showing AFM force curve obtained from the measurement of the cantilever deflection.

DOI: 10.1021/acsomega.9b01491
ACS Omega 2019, 4, 13319−13329

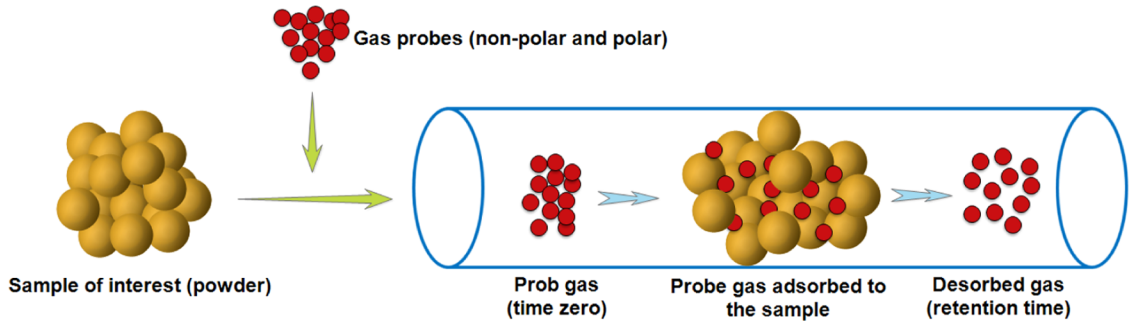

Figure 6. Schematic showing the principle of inverse gas chromatography (IGC) for surface energy measurement.

$$W_{ll} = \gamma_l + \gamma_l - 0 = 2\gamma_l \quad (5)$$

Based on Berthelot's assumption, the adhesion work between the solid and liquid W_{sl} is equal to the geometric mean of the cohesion work of a solid and liquid individually

$$W_{sl} = (W_{ss}W_{ll})^{1/2} \quad (6)$$

Combining the eqs 3−6 results in eq 7, which is the basis of surface energy calculations

$$W_{sl} = 2(\gamma_s\gamma_l)^{1/2} = \gamma_l(1 + \cos\theta) \quad (7)$$

Several models and approaches have been developed based on the contact angle measurement to derive the expressions for surface energy calculation. These models are based on different viewpoints; however, none of them is universal and ideally match the reality. Since the surface energy of a mineral is not an exact and absolute value, five commonly accepted models, Fowkes, Van Oss−Chaudhury−Good, Owens−Wendt−Rabel−Kaelble, Zisman, and Neumann models, were used in this study to calculate the surface energy of rare earth minerals from contact angle data. Authors believe that this approach could provide more reliable information on the polar and nonpolar components of the surface energy of bastnaesite and xenotime.

2.2.2.3. Surface Energy Analysis by Atomic Force Microscopy. The interaction between the AFM tip and the mineral substrate was analyzed by measuring the deflection of the cantilever. The force curves were obtained by plotting the cantilever's deflection against the distance of the tip from the sample. Force curves were used to evaluate the forces applied to the surface and compare the type of interactions taking place on the mineral surfaces. Figure 5a schematically shows the deflection of the cantilever as well as the tip and the cantilever used in this paper.

In Figure 5b, a scheme of the force curve is presented. As shown, two plots were obtained from the measurement of cantilever deflection. In the region 1−2, there was no interaction between the tip and the solid surface since the tip was not close enough to the solid surface. As the tip approached the sample, the tip was pulled down in the region 2−3 due to the attraction forces. The cantilever bent upward in the region 3−4 as the tip passed into the surface. In the region 4−5, the tip retracted, and cantilever began to relax until the tip force got in equilibrium with the forces on the surface of the sample. In region 5−6, retraction continued, and the cantilever bent downward as the sample surface tried to attract the tip. There was no interaction in region 7−8 as the tip was completely separated.

In this paper, the force curves were plotted for both bastnaesite and xenotime to obtain the work of adhesion and qualitatively compare the surface energy of the two minerals. The instrument was operated in the contact mode to measure the positive deflection of the cantilever. The pull-off force (adhesion force) was calculated using Hooke's law, $F = KZ$, where K is the spring constant of the cantilever and Z is the deflection of the cantilever during the contact between the tip and mineral surfaces. Then two models of contact mechanics (Deryaguin−Muller−Toporov[36] and Johnson−Kendall−Roberts[37]) were employed to convert the pull-off force into the work of adhesion.

2.2.2.4. Surface Energy Analysis by Inverse Gas Chromatography. IGC is a physicochemical, gas−solid technique for the determination of surface and bulk properties of powders and particulates. A schematic showing the principle of inverse gas chromatography (IGC) for surface energy measurement is presented in Figure 6. The vapor probes with known properties were passed through the chromatography column packed with the mineral powder. A series of nonpolar probes (*n*-alkanes) were injected, and their retention time was measured. The retention time was a result of adsorption and desorption of the probe molecules on the mineral surface. The probe molecules desorbed from the mineral surface were detected by the flame ionization detector, and the retention time was determined. The retention time was then converted to the surface energy by applying the Dorris−Gray and Schultz approaches.[38,39] The relationship between the retention volume and dispersive component of surface energy can be determined using eq 8

$$RT\ V_R^0 = 2N_A(\gamma_S^D)^{1/2}a(\gamma_l^D)^{1/2} + \text{constant} \quad (8)$$

where R is the gas constant, T is the absolute temperature, V_R^0 is the retention volume, N_A is the Avogadro's constant, and a is the cross-sectional area of the probe molecule. The retention volume is determined from the retention time using eq 9.

$$V_R^0 = \frac{j}{m}\cdot F\cdot(t_R - t_0)\cdot\frac{T}{273.15} \quad (9)$$

where j is the James−Martin pressure correction factor, which corrects the retention time and makes the retention volume independent of pressure, m is the mass of sample, F is the exit flow rate, t_R is the retention time for the adsorbing probe, t_0 is the hold-up time of the mobile phase, and T is the temperature of the column.

If the left side of eq 8 is plotted versus $a(\gamma_l^D)^{1/2}$ for a series of alkanes, the slope of the straight line will allow the calculation of dispersive component of surface energy. To determine the acid−base component, polar probe molecules were injected.

DOI: 10.1021/acsomega.9b01491
ACS Omega 2019, 4, 13319−13329

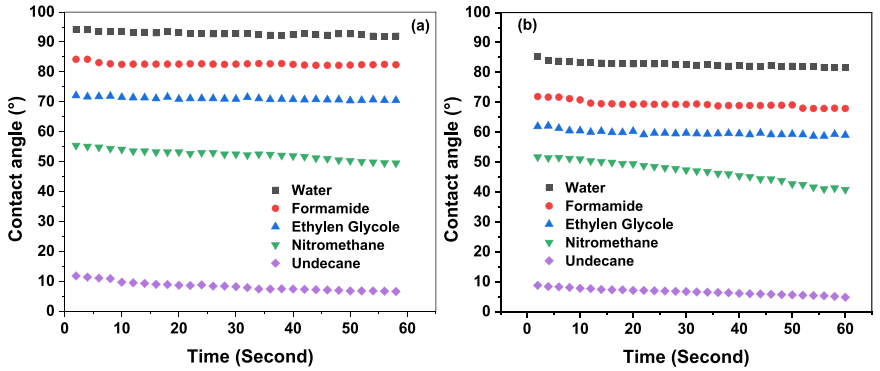

Figure 7. Advancing contact angles of probe liquids as a function of time for (a) bastnaesite and (b) xenotime.

The data points related to the polar probe molecules were located beyond the alkane line. The vertical distance between the polar points and alkane line represents the specific component of the Gibbs free energy, ΔG. The electron-acceptor and -donor values were obtained from the Gibbs free energy by applying the Good-van Oss concept (eq 10), and then the acid–base component was estimated by using the geometric mean of the γ_S^+ and γ_S^- parameters (eq 11).

$$\Delta G = N_A \cdot \alpha \cdot 2 \cdot ((\gamma_L^+ \cdot \gamma_S^-)^{1/2} + (\gamma_L^- \cdot \gamma_S^+)^{1/2}) \quad (10)$$

$$\gamma_S^{AB} = 2 \cdot \sqrt{\gamma_S^+ \cdot \gamma_S^-} \quad (11)$$

3. RESULTS AND DISCUSSION

The values of the contact angle of probe liquids on mineral surfaces were plotted as a function of time from 0 to 60 s (Figure 7), and the relative equilibrium contact angle was used to calculate the surface energy of rare earth minerals. As shown in Figure 7, the contact angle values of all liquids on bastnaesite were greater than those on xenotime. Unlike water, the contact angle of formamide decreased as time increased due to the stronger bonding mechanism, which reduced the interfacial energy through acid–base interactions. Undecane is a nonpolar liquid that has a lower surface tension, which resulted in a smaller contact angle in comparison with polar probes. Contact angle values obtained with nitromethane for bastnaesite and xenotime were close to each other, and the contact angle values obtained with undecane were similar for both rare earth minerals.

Even though the result of contact angle measurements may vary depending on the experimental methodology, this technique is widely accepted for comparative assessment of surface properties of solid materials. In this study, contact angle values were used to analyze the surface energy of bastnaesite and xenotime by the means of Fowkes, Van Oss–Chaudhury–Good, Owens–Wendt–Rabel–Kaelble, Zisman, and Neumann models.

According to the Fowkes model,[12] the surface energy of solids and liquids can be dissociated to the independent components. Fowkes theory assumes that the total surface energy of a solid is the sum of the polar and dispersive (nonpolar) components

$$\gamma_s = \gamma_s^d + \gamma_s^p \quad (12)$$

where d and p are the dispersive and polar components, respectively. Combining eqs 7 and 12 makes it possible to express the work of adhesion, yielding the surface energy components

$$\frac{\gamma_l(1 + \cos\theta)}{2} = (\gamma_l^d)^{1/2}(\gamma_s^d)^{1/2} + (\gamma_l^p)^{1/2}(\gamma_s^p)^{1/2} \quad (13)$$

Figure 8 shows the values of the surface free energy and its dispersive and polar components obtained from Fowkes model

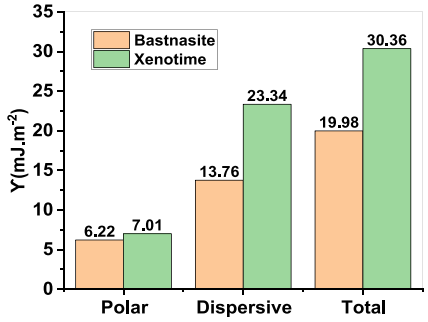

Figure 8. Polar, dispersive, and total surface energy of rare earth minerals obtained by the Fowkes model.

for rare earth minerals. As it is shown, the dispersive portion was much larger than nondispersive part for both bastnaesite and xenotime. The dispersive portion was due to London forces, which resulted from instantaneous dipole-induced dipole forces. The London dispersion forces are always present in all types of materials and take place at the liquid–solid interfaces, even though the dispersive forces might be weaker than other intermolecular forces. Dispersive energy of the xenotime was larger than that of bastnaesite, whereas the polar components were close to each other. This observation was a result of the difference in the ionization energies of elements on bastnaesite and xenotime surfaces, which would influence their surfaces' reactivity. The polar component results from Coulomb interactions between permanent dipoles, permanent dipoles and induced dipoles. In fact, if two phases, which are in contact, have an equal or similar ratio of dispersive to polar components, the interaction between two phases will be larger.

The Fowkes theory is based on the additivity of the polar (acid–base) and apolar (Lifshitz–van der Waals) interactions. However, the electron-acceptor and electron-donor constituents of the polar component of the surface energy are not additive.

Van Oss, Chaudhury proposed another approach to include the hydrogen-bond interactions in the surface energy calculations.[40] According to vOCG model, the surface energy

DOI: 10.1021/acsomega.9b01491
ACS Omega 2019, 4, 13319–13329

consists of apolar component (wherein Lifshitz–van der Waals interactions including dispersion and induced dipole–dipole interactions take place) and polar component (wherein Lewis acid–base interactions including hydrogen-bond interactions take place). The equation proposed by vOCG model for solid and liquid surface energies is

$$\gamma_l(1 + \cos\theta) = 2(\gamma_s^{lw}\gamma_l^{lw})^{1/2} + 2(\gamma_s^{+}\gamma_l^{-})^{1/2} + 2(\gamma_s^{-}\gamma_l^{+})^{1/2} \quad (14)$$

Figure 9 shows the values of electron-donor and electron-acceptor parameters as well as apolar (Lifshitz–van der Waals)

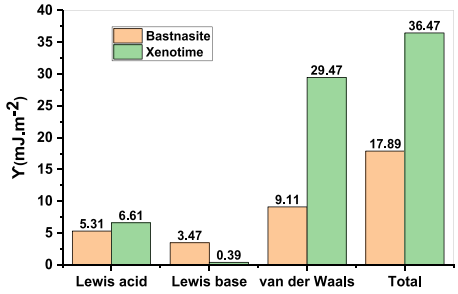

Figure 9. Polar (acid–base) and apolar (Lifshitz–van der Waals) components of the surface energy of rare earth minerals obtained by Van Oss–Chaudhury–Good model.

component of the surface energy for both bastnaesite and xenotime. As shown in Figure 9, the Lifshitz–van der Waals interactions for xenotime were about three times greater than that of bastnaesite. The electron-donor parameter (Lewis base, γ^-) value of xenotime was close to zero, whereas its electron-acceptor parameter (Lewis acid, γ^+) was 6.6 mJ m^{-2}. According to the vOCG model, although the xenotime surface seemed to be monopolar, the bastnaesite had a bipolar surface. The results obtained by Van Oss–Chaudhury–Good model confirmed that the acid–base interactions between rare earth minerals and tested probe liquids were small, and the Lifshitz–van der Waals interactions dominated. However, the calculated values of surface energy components may vary depending on the choice of probe liquids.

Owens, Wendt, Rabel, and Kaelble considered the geometric mean of the dispersive and nondispersive parts of the solid and liquid surface energies[41−43]

$$\gamma_{sl} = \gamma_s + \gamma_l - 2(\gamma_s^d\gamma_l^d)^{1/2} - 2(\gamma_s^p\gamma_l^d)^{1/2} \quad (15)$$

Substituting eq 15 in Young's equation yields

$$\frac{\gamma_l(1 + \cos\theta)}{2(\gamma_l^d)^{1/2}} = (\gamma_s^p)^{1/2}\frac{(\gamma_l^p)^{1/2}}{(\gamma_l^d)^{1/2}} + (\gamma_s^d)^{1/2} \quad (16)$$

Dispersive and polar components of the surface energy of rare earth minerals were evaluated by plotting the left side of eq 16 versus $\frac{(\gamma_l^p)^{1/2}}{(\gamma_l^d)^{1/2}}$. Creating the linear regression of the data and the determination of slope and Y-intercept allowed to determine the polar and dispersive portions of surface energy, respectively. In the case of solids having a low polar part, the amount of $(\gamma_s^p\gamma_l^p)^{1/2}$ will be reduced, and, consequently, the contribution of the polar interactions will decrease.

Figure 10 shows the polar and dispersive energies of bastnaesite and xenotime obtained by the OWRK method. The dispersive energies of bastnaesite and xenotime obtained by this method were relatively equal. Both polar and dispersive energies of xenotime obtained by OWRK model were close to those calculated by Fowkes model. In fact, the assumptions made in these two models are similar. The OWRK and Fowkes models are mathematically identical, but the way that the OWRK model uses for surface energy calculation is based on the graphical evaluation. However, in the case of bastnaesite, the dispersive energy obtained by OWRK model was larger than that calculated by Fowkes model, whereas the polar surface energy was smaller. According to the surface energy values obtained by Van Oss–Chaudhury–Good model, the polar energy of the rare earth minerals was small, so the $(\gamma_s^p\gamma_l^p)^{1/2}$ in the OWRK model assumed a low value. Hence, the polar interactions had a small contribution to the interfacial tension between the rare earth minerals and the probe liquids. The polar component in the OWRK model accounts for site-specific interactions such as hydrogen bonding and Coulomb interactions between dipoles (dipole–dipole and dipole-induced dipole). The OWRK model has been proven to provide acceptable results for different solid surfaces, however, it has also been reported that this model is unable to cover all of the nondispersive interactions.

Although the dispersive component exists in all models developed for surface energy calculations, the definition and origin of the second component are still under debate. Neumann's equation of state addressed this challenge by not separating the surface energy into several interactions.[44] Neumann et al. assumed that the interfacial energy between solid and liquid, γ_{sl}, depends only on the surface energy of the solid and the liquid. The formula based on Neumann's

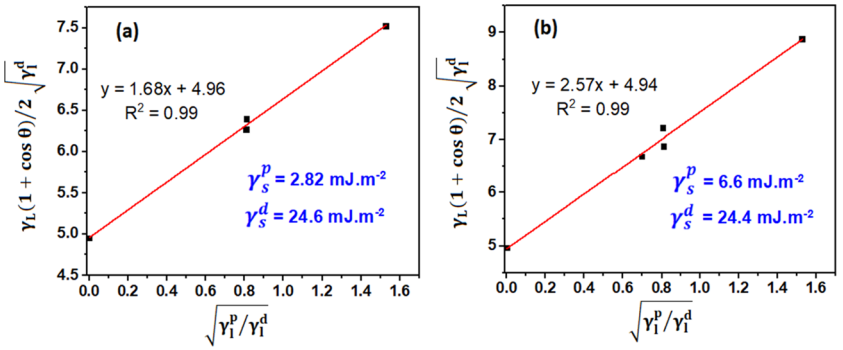

Figure 10. Polar and dispersive components of the surface energy of (a) bastnaesite; (b) xenotime obtained by the Owens–Wendt–Rabel–Kaelble model.

DOI: 10.1021/acsomega.9b01491
ACS Omega 2019, 4, 13319−13329

equation of state expresses the relation between contact angle, solid surface energy, and liquid surface energy as follows

$$\gamma_l(1 + \cos\theta) = 2\sqrt{\gamma_s\gamma_l}[1 - \beta(\gamma_l - \gamma_s)^2] \quad (17)$$

where β is a modification constant to address the errors made by unlike-pair interactions between solid and liquid. The total surface energy of bastnaesite and xenotime was determined by solving the eq 17 for each probe liquid. In Table 2, the total surface energy of rare earth minerals calculated by Neumann's equation of state is presented. As it is seen, the surface energy values of bastnaesite and xenotime were in the range of 22−29 and 24−35 mJ m^{-2}, respectively. Neumann's model is controversial due to not considering the statistical thermodynamics and origin of the molecules, which are the basis for the geometric approach. Each probe liquid gives unique surface energy, which does not include the dispersive and polar components; however, the Neumann's model well indicated how the probe liquid can affect the surface energy value. In fact, the competition between the solid−liquid adhesive forces and cohesive interactions in the probe liquid determines the shape of the drop and, thus, contact angle value.

Table 2. Surface Energy of Bastnaesite and Xenotime Obtained by Neumann's Model for Different Probe Liquids (β = 0.00012)

	total surface energy (mJ m^{-2})	
probe liquid	bastnaesite	xenotime
water	28.8	34.6
formamide	26	34.5
ethylene glycol	24.7	30.7
nitromethane	25.3	28.9
undecane	22.6	24.7

Other than Neumann's equation of state, the Zisman model is also another one-parameter model.[45] According to Zisman's theory, the surface energy of a solid is simply equal to the surface energy of the liquid that can completely wet the solid surface and make a contact angle of 0^0. This is due to the fact that the contact angle decreases as the surface energy of liquid decreases. The contact angle data for five probe liquids on rare earth minerals was acquired, and then the cosine of contact angle values ($\cos\theta$) against known surface energy of probe liquids was plotted and extrapolated to $\cos\theta = 1$ ($\theta = 0^0$). In Figure 11, the Zisman plots for bastnaesite and xenotime are shown. The Zisman plot shows that the surface energies of bastnaesite and xenotime were 23.8 and 22 mJ m^{-2}, respectively. It should be noted that the energy obtained by the Zisman method is called "critical surface energy", which is different from the surface energy γ_s, calculated by other methods. The Zisman's critical surface energy is assumed to be equal to the surface tension of the liquid, which makes zero contact angle with the solid surface. In fact, the Zisman method works better for nonpolar surfaces and is inadequate for the surfaces such as rare earth minerals, which have some polar energies as well.

Despite all of the advantages of the contact angle measurement technique, the surface energy calculated by the relevant models is dependent on the selected probe liquids. Atomic force microscopy has been recently used to measure the tip−substrate forces to determine the surface energy without the interference of probe liquids. In this paper, the same planes of bastnaesite and xenotime used for contact angle studies were used for the AFM analysis. The measurements were conducted at ambient conditions and controlled humidity. The pull-off force depends on the probe size and the tip radius, which determine the contact area. The length of the probe was ≈450 μm and the width was 50 μm. The tip had a pyramidal shape with a curvature radius 10 nm. A typical force−distance curve obtained for the {100} faces of rare earth minerals using a silicon nonfunctionalized tip is shown in Figure 12. The approach curve was flat for both rare earth minerals until the long-range forces were absent, and jump-to contact was reached. The tip jumped to contact on xenotime surface when the tip−surface distance was about 2370 nm, whereas this value was about 2250 nm for bastnaesite. A slight sublinearity was observed, possibly indicating an elastic deformation of the crystals. After the tip jumps to contact, the repulsive interaction took place, and as the tip moved inward, the cantilever started to bend. The maximum deflections of the cantilever were ≈1460 and 1150 nm for xenotime and bastnaesite, respectively. As the cantilever retracted the reverse phenomenon took place and finally the tip jumped off the surface when the spring force of the cantilever overcame the tip−mineral adhesion force. The pull-off force was calculated based on Hook's law and the jump-off contact minimum. The pull-off forces obtained for xenotime and bastnaesite were 24 and 15 nN, respectively. Two contact mechanics models, Johnson−Kendall−Roberts (JKR) and Deryaguin−Muller−Toporov (DMT), were employed to convert the pull-off force to the work of adhesion. The work of adhesion is directly proportional to the surface energy of the rare earth minerals. According to JKR model, the pull-off force (F) is correlated with the work of adhesion (W_A) by

$$F = \frac{3}{2}\pi R W_A \quad (18)$$

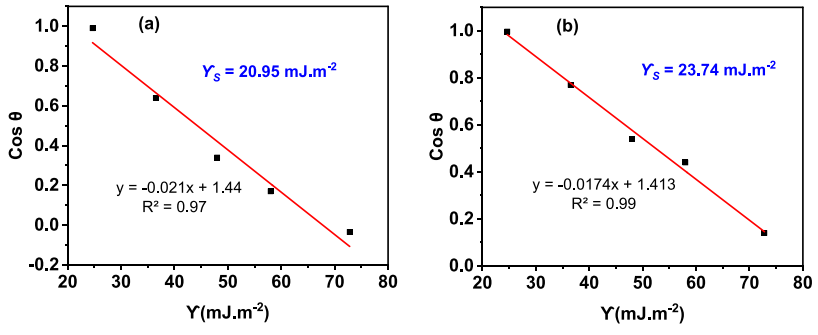

Figure 11. Surface energy of (a) bastnaesite and (b) xenotime obtained by the Zisman model.

DOI: 10.1021/acsomega.9b01491
ACS Omega 2019, 4, 13319−13329

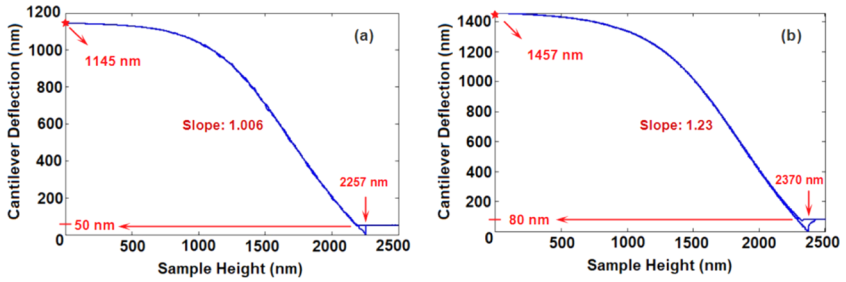

Figure 12. Force curves showing the interactions between the AFM probe and (a) bastnaesite surface and (b) xenotime surface.

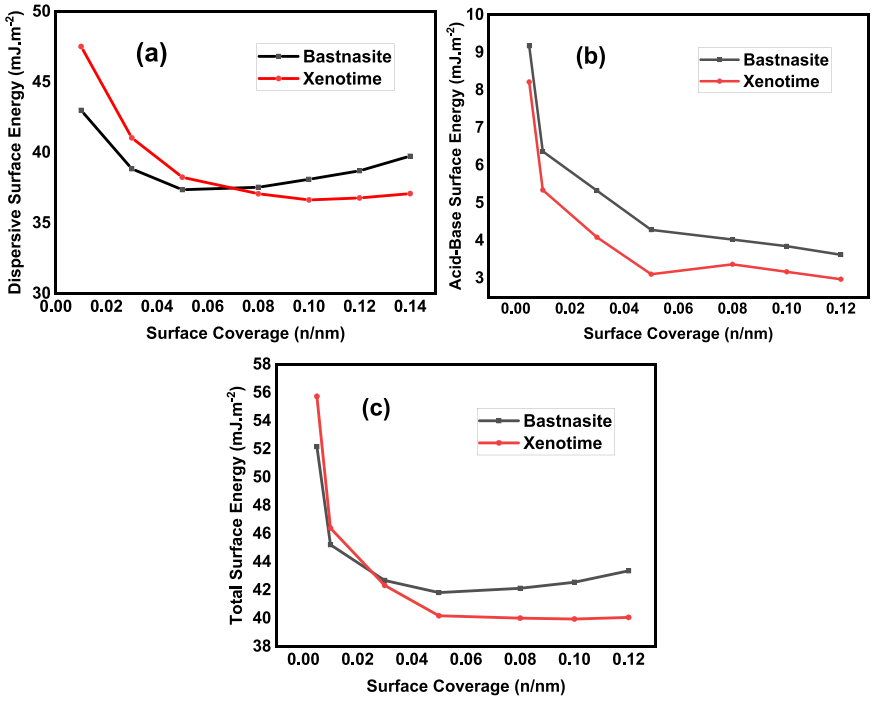

Figure 13. (a) Dispersive, (b) acid−base, and (c) total surface energy profile of rare earth minerals obtained from the IGC analysis.

according to the DMT model, the pull-off force is given as

$$F = 2\pi R W_A \tag{19}$$

where R is the radius of the probe tip.

The work of adhesion obtained by JKR and DMT models for xenotime was 1.6 times higher than that calculated for bastnaesite, which was comparable with the results obtained by Fowkes and OWRK models used in the contact angle measurements. However, the AFM technique, in this study, was only used for qualitative analysis and comparison of rare earth minerals' wettability since the surface energy values obtained by AFM technique should be regarded with caution due to the inconsistency and irreproducibility of the results. The variation in surface roughness and heterogeneity characteristics as well as the probe imperfection caused irreproducibility of the surface energy values.

Mineral surfaces are usually heterogeneous, therefore a single value for surface energy cannot represent the whole surface. Inverse gas chromatography (IGC) was employed to get more information on the underlying heterogeneity of the rare earth minerals to provide a more realistic surface energetics data. Although the contact angle measurements and the atomic force microscopy were applied on the rare earth crystalline faces, the IGC analysis was applied on the rare earth mineral powders. The surface energies for both bastnaesite and xenotime were calculated at identical coverages from 0.01 to 0.15 n/nm. Figure 13 shows the profile of dispersive surface energy, specific (acid−base) surface energy, and total surface energy for rare earth minerals measured by the IGC technique. It is observed that the surface energy of both minerals decreased as the surface coverage increased; however, the variation of surface energy values was not large. As shown in Figure 13a, the dispersive surface energy of xenotime was greater than that of bastnaesite within the surface coverages 0.01−0.05 n/n_m, then they became closer as the surface coverages increased. The dispersive surface energy for xenotime was in the range of 37−48 mJ m^{-2} and for bastnaesite was in the range of 37−43 mJ m^{-2}, which are obviously larger than what obtained by contact angle measurements and relative models. In fact, the higher energy sites made a larger contribution in comparison with the lower energy sites of the mineral surfaces; therefore, the dispersive energy obtained by IGC was higher compared to the values achieved by the contact angle measurements.

The specific component of surface energy, also called acid−base contribution to the surface energy, was determined by measuring the retention time of dichloromethane (monopolar Lewis acid) and ethyl acetate (monopolar Lewis base), As

DOI: 10.1021/acsomega.9b01491
ACS Omega 2019, 4, 13319−13329

shown in Figure 13b, the acid−base surface energy of bastnaesite was larger than that of xenotime, which was in agreement with the results obtained by the vOCG model used in the contact angle measurement study. According to the IGC results, the acid−base surface energy for xenotime was in the range of 3−8 mJ m^{-2} and for bastnaesite was in the range of 3.5−9 mJ m^{-2}. Acid−base surface interactions are comprised of electron-acceptor (Lewis acid) and electron-donor (Lewis base) parameters. Based on the vOCG model used in contact angle measurements and the geometric mean of the γ_S^+ and γ_S^- parameters, the γ^{AB} for bastnaesite was 8.6 mJ m^{-2} and for xenotime was 3.2 mJ m^{-2}. However, the contact angle measurements and the vOCG model demonstrated that the Lewis acidic portion made a larger contribution to the specific component of the surface energy of xenotime.

4. CONCLUSIONS

Surface energy and wettability of bastnaesite and xenotime, as major commercial sources of heavy and light rare earth elements, were investigated and compared using a combination of techniques including contact angle measurement, atomic force microscopy, and inverse gas chromatography. Contact angle-based models revealed notable differences in dispersive and polar surface energy constituents of rare earth minerals. The results obtained by these models were dependent on the type of probe liquid used. However, surface roughness, local properties, and composition variation seemed to have a greater impact on the surface energy analysis of the two minerals studied. According to contact angle measurements, bastnaesite exhibited a more hydrophobic character and had relatively smaller total and dispersive surface energy values. The assumptions made in Fowkes and OWRK models are similar; however, the results obtained by these two models were slightly different. In the OWRK model, the surface energy values were calculated based on the graphical evaluation. Both polar and dispersive energies of xenotime obtained by OWRK model were close to those calculated by Fowkes model, but in the case of bastnaesite, the dispersive energy obtained by OWRK model was larger than that calculated by Fowkes model, whereas the polar surface energy was smaller. Results obtained using Zisman model showed that this model is inadequate for probing mineral surfaces with polar characteristics. Neumann's equation of state, a one-parameter model, showed better performance for the mineral surfaces when polar probes were used for calculations. In the vOCG model, the hydrogen-bond interactions were included in the surface energy calculations. Based on this model, xenotime displayed a smaller acid−base surface energy, which was in agreement with IGC results. The work of adhesion obtained from the force curve analysis revealed a higher wettability for xenotime, supporting the results achieved by contact angle measurements. The specific and nonspecific surface energy of bastnaesite and xenotime were measured by inverse gas chromatography to take the surface heterogeneity into consideration. IGC results showed a relatively higher dispersive surface energy values in comparison with contact angle measurements due to the larger contribution of higher energy sites in IGC technique. However, the polar surface energy obtained by IGC technique was relatively close to those calculated by contact angle models. It should be noted that the complexity of the polar and nonpolar interfacial interactions makes it very difficult to provide a secure basis for getting a simple conclusion on the surface energy of rare earth minerals. This paper demonstrates that using a single technique cannot provide reliable data on the surface energy of minerals, but using a combination of techniques and models gives a better understanding of surface chemistry of solid materials.

AUTHOR INFORMATION

Corresponding Author

*E-mail: alaghal@mst.edu. Phone: 573-341-6287. Fax: 573-341-6934.

ORCID

Lana Alagha: 0000-0001-7481-8663

Notes

The authors declare no competing financial interest.

ACKNOWLEDGMENTS

The authors gratefully acknowledge the financial support provided by the Center for Research in Energy and Environment (CREE) at Missouri University of Science and Technology.

REFERENCES

(1) Becker, U.; Rosso, K. M.; Hochella, M. F. The proximity effect on semiconducting mineral surfaces: a new aspect of mineral surface reactivity and surface complexation theory? *Geochim. Cosmochim. Acta* **2001**, *65*, 2641−2649.

(2) Planinšek, O.; Pišek, R.; Trojak, A.; Srčič, S. The utilization of surface free-energy parameters for the selection of a suitable binder in fluidized bed granulation. *Int. J. Pharm.* **2000**, *207*, 77−88.

(3) Somasundaran, P.; Zhang, L. Adsorption of surfactants on minerals for wettability control in improved oil recovery processes. *J. Pet. Sci. Eng.* **2006**, *52*, 198−212.

(4) Srinivasan, S. G.; Shivaramaiah, R.; Kent, P. R. C.; Stack, A. G.; Riman, R.; Anderko, A.; Navrotsky, A.; Bryantsev, V. S. A comparative study of surface energies and water adsorption on Ce-bastnäsite, La-bastnäsite, and calcite via density functional theory and water adsorption calorimetry. *Phys. Chem. Chem. Phys.* **2017**, *19*, 7820−7832.

(5) Mohammadi-Jam, S.; Burnett, D. J.; Waters, K. E. Surface energy of minerals − Applications to flotation. *Miner. Eng.* **2014**, *66−68*, 112−118.

(6) Alsafasfeh, A.; Khodakarami, M.; Alagha, L.; Moats, M.; Molatlhegi, O. Selective Depression of Silicates in Phosphate Flotation Using Polyacrylamide-Grafted Nanoparticles. *Miner. Eng.* **2018**, *127*, 198−207.

(7) Khodakarami, M.; Molatlhegi, O.; Alagha, L. Evaluation of Ash and Coal Response to Hybrid Polymeric Nanoparticles in Flotation Process: Data Analysis Using Self-Learning Neural Network. *Int. J. Coal Prep. Util.* **2019**, *39*, 199−218.

(8) Drummond, C.; Israelachvili, J. Surface forces and wettability. *J. Pet. Sci. Eng.* **2002**, *33*, 123−133.

(9) Blake, T.; Coninck, J. D. The influence of solid-liquid interactions on dynamic wetting. *Adv. Colloid Interface Sci.* **2002**, *96*, 21−36.

(10) Kozbial, A.; Li, Z.; Conaway, C.; Mcginley, R.; Dhingra, S.; Vahdat, V.; Zhou, F.; D'Urso, B.; Liu, H.; Li, L. Study on the Surface Energy of Graphene by Contact Angle Measurements. *Langmuir* **2014**, *30*, 8598−8606.

(11) Bikermann, J. J. Surface energy of solids. *Top. Curr. Chem.* **1978**, *77*, 1−66.

(12) Fowkes, F. M. Attractive forces at interfaces. *Ind. Eng. Chem.* **1964**, *56*, 40−52.

(13) Kaelble, D. H. Dispersion-polar surface tension properties of organic solids. *J. Adhes.* **1970**, *2*, 66−81.

(14) Oss, C. J. V.; Good, R. J.; Chaudhury, M. K. Additive and Non-additive Surface Tension Components and the Interpretation of Contact Angles. *Langmuir* **1988**, *4*, 884−891.

DOI: 10.1021/acsomega.9b01491
ACS Omega 2019, 4, 13319−13329

(15) Law, K.-Y.; Zhao, H. *Surface Wetting: Characterization, Contact Angle, and Fundamentals*; Springer: Cham, 2016.
(16) El-Hefian, E. A.; Yahaya, A. H. Investigation on Some Properties of SDS Solutions. *Aust. J. Basic Appl. Sci.* **2011**, *5*, 1221−1227.
(17) Park, J. K.; Ryu, J.; Koo, B. C.; Lee, S.; Kang, K. H. How the change of contact angle occurs for an evaporating droplet: effect of impurity and attached water films. *Soft Matter* **2012**, *8*, 11889−11896.
(18) Chau, T. A review of techniques for measurement of contact angles and their applicability on mineral surfaces. *Miner. Eng.* **2009**, *22*, 213−219.
(19) Amrei, M.; Davoudi, M.; Chase, G.; Tafreshi, H. V. Effects of roughness on droplet apparent contact angles on a fiber. *Sep. Purif. Technol.* **2017**, *180*, 107−113.
(20) Woodward, J. T.; Gwin, H.; Schwartz, D. K. Contact Angles on Surfaces with Mesoscopic Chemical Heterogeneity. *Langmuir* **2000**, *16*, 2957−2961.
(21) Mohammadi-Jam, S.; Waters, K. E. Inverse gas chromatography applications: A review. *Adv. Colloid Interface Sci.* **2014**, *212*, 21−44.
(22) Newell, H. E.; Buckton, G. Inverse Gas Chromatography: Investigating Whether the Technique Preferentially Probes High Energy Sites for Mixtures of Crystalline and Amorphous Lactose. *Pharm. Res.* **2004**, *21*, 1440−1444.
(23) Leite, F. L.; Bueno, C. C.; Róz, A. L. D.; Ziemath, E. C.; Oliveira, O. N. Theoretical Models for Surface Forces and Adhesion and Their Measurement Using Atomic Force Microscopy. *Int. J. Mol. Sci.* **2012**, *13*, 12773−12856.
(24) Hong, G.; Choi, J.; Han, Y.; Yoo, K.-S.; Kim, K.; Kim, S. B.; Kim, H. Relationship between Surface Characteristics and Floatability in Representative Sulfide Minerals: Role of Surface Oxidation. *Mater. Trans.* **2017**, *58*, 1069−1075.
(25) Shackleton, N.; Malysiak, V.; Oconnor, C. Surface Characteristics and Flotation Behaviour of Platinum and Palladium Arsenides. *Int. J. Miner. Process.* **2007**, *85*, 25−40.
(26) Fuerstenau, M.; Sabacky, B. On the Natural Floatability of Sulfides. *Int. J. Miner. Process.* **1981**, *8*, 79−84.
(27) Miller, J. D.; Wang, X.; Jin, J.; Shrimali, K. Interfacial Water Structure and the Wetting of Mineral Surfaces. *Int. J. Miner. Process.* **2016**, *156*, 62−68.
(28) Yin, X.; Gupta, V.; Du, H.; Wang, X.; Miller, J. D. Surface charge and wetting characteristics of layered silicate minerals. *Adv. Colloid Interface Sci.* **2012**, *179*−*182*, 43−50.
(29) Miller, J. D.; Nalaskowski, J.; Abdul, B.; Du, H. Surface characteristics of kaolinite and other selected two layer silicate minerals. *Can. J. Chem. Eng.* **2007**, *85*, 617−624.
(30) Nalaskowski, J.; Abdul, B.; Du, H.; Miller, J. D. Anisotropic character of talc surfaces as revealed by streaming potential measurements, atomic force microscopy, molecular dynamics simulations and contact angle measurements. *Can. Metall. Q.* **2007**, *46*, 227−235.
(31) Jordens, A.; Marion, C.; Kuzmina, O.; Waters, K. E. Surface Chemistry Considerations in the Flotation of Bastnasite. *Miner. Eng.* **2014**, *66*−*68*, 119−29.
(32) Zhang, X.; Du, H.; Wang, X.; Miller, J. D. Surface Chemistry Considerations in the Flotation of Rare-Earth and Other Semisoluble Salt Minerals. *Miner. Metall. Process.* **2013**, *30*, 24−37.
(33) Zhang, Y. Froth flotation of xenotime. MS Thesis, Kroll Inst. Extr. Metall., Colo. School Mines, 2016.
(34) Young, T. An essay on the cohesion of fluids. *Philos. Trans. R. Soc. London* **1805**, *95*, 65−87.
(35) Dupre, M. A. *Theorie mechanique de la chaleur*; Gauthier-Villars: Pairs, 1869.
(36) Derjaguin, B. V.; Muller, V. M.; Toporov, Y. P. Effect of contact deformations on the adhesion of particles. *J. Colloid Interface Sci.* **1975**, *53*, 314−326.
(37) Johnson, K. L.; Kendall, K.; Roberts, A. D. Surface energy and the contact of elastic solids. *Proc. R. Soc. A* **1971**, *324*, 301−313.
(38) Dorries, G. M.; Gray, D. G. Adsorption of n-alkanes at zero surface coverage on cellulose paper and wood fibers. *J. Colloid Interface Sci.* **1980**, *77*, 353−362.
(39) Schultz, J.; Lavielle, L.; Martin, C. The Role of the Interface in Carbon Fibre-Epoxy Composites. *J. Adhes.* **1987**, *23*, 45−60.
(40) Oss, C. V.; Good, R.; Chaudhury, M. The Role of van der Waals Forces and Hydrogen Bonds in "Hydrophobic Interactions" between Biopolymers and Low Energy Surfaces. *J. Colloid Interface Sci.* **1986**, *111*, 378−390.
(41) Owens, D. K.; Wendt, R. C. Estimation of the Surface Free Energy of Polymers. *J. Appl. Polym. Sci.* **1969**, *13*, 1741−1747.
(42) Kaelble, D. H. Dispersion-Polar Surface Tension Properties of Organic Solids. *J. Adhes.* **1970**, *2*, 66−81.
(43) Rabel, W. Einige Aspekte der Benetzungstheorie und ihre Anwendung auf die Untersuchung und Veränderung der Oberflächeneigenschaften von Polymeren. *Farbe Lack* **1971**, *77*, 997−1005.
(44) Neumann, A.; Good, R.; Hope, C.; Sejpal, M. An equation-of-state approach to determine surface tensions of low-energy solids from contact angles. *J. Colloid Interface Sci.* **1974**, *49*, 291−304.
(45) Zisman, W. A. Relation of the Equilibrium Contact Angle to Liquid and Solid Constitution. *Adv. Chem.* **1964**, *43*, 1−51.

DOI: 10.1021/acsomega.9b01491
ACS Omega 2019, 4, 13319−13329